

Examination of the processes of deformation and fracture in a silica-filled epoxy resin

W. J. CANTWELL, J. W. SMITH, H. H. KAUSCH

Laboratoire de Polymères, Ecole Polytechnique Fédérale de Lausanne, Ch. de Bellerive 32, 1007 Lausanne, Switzerland

T. KAISER

Corporate Research, ASEA Brown Boveri and Cie, CH-5405 Baden, Switzerland

A series of short-term fracture tests have been undertaken on a silica-filled epoxy resin in order to examine the processes of damage initiation, development and fracture in a particulate-filled polymer. Several different types of inelastic deformation and fracture mechanisms were observed within the volume of the material. These included localized shear yielding, particle-matrix debonding and micro-cracking. The relative amount of each of these was found to depend upon the test rate and temperature. At low temperatures and high rates of loading, failure was associated with one single debonding event whereas at high temperatures and low rates, debonding and yielding were found to be extensive throughout the volume of the test specimens. A detailed examination of the fractured specimens identified several distinct regions on the fracture surface. Surrounding the defect the particles were often debonded from the matrix suggesting that the crack had propagated in a sub-critical manner. Beyond this zone was a smooth zone corresponding to the region over which the crack was accelerating unstably. The smooth zone then developed into a rough three-dimensional zone in which the crack was propagating at its maximum velocity. The size of each of these zones was found to vary considerably with test temperature and cross-head speed.

1. Introduction

The addition of a rigid particulate filler such as silica flour to epoxy resin serves to reduce costs as well as to enhance certain mechanical properties such as the Young's modulus, fracture toughness and high-temperature load-bearing capability. Detailed examinations of the mechanisms of damage initiation in these materials are few and a complete explanation of the processes occurring during deformation and fracture within these materials is still sought. Conversely, much work has been undertaken on unfilled epoxy resins and here a reasonably clear understanding of the failure processes has been achieved. Following some initial disagreement, it is now generally accepted that shear yielding is the primary mechanism for non-elastic deformation in epoxy resins. The limited evidence for crazing in these materials [1, 2] is not strong and certainly no clear fibrillar structures similar to those seen in many thermoplastic materials have been observed.

The large number of fractographic analyses of epoxy resins have yielded an equally large number of terms to describe the fracture surface features, these include, fish-eye patterns [3], furrows [4], river markings [4], steps [5] and tracks [6]. Wronski and Parry [7], following a series of tensile tests on a plasticized epoxy, identified three distinct zones on the fracture surfaces of the failed specimens. The first, a relatively flat semi-elliptical zone, was assumed to correspond to

the region of sub-critical crack growth. This was superceded by a very smooth featureless area and a somewhat rougher three-dimensional zone exhibiting a series of almost parallel linear features termed rib markings. No clear explanation was offered regarding the formation of the second and third zones. Similar features were observed by Koga *et al.* [8] following fatigue tests on two different epoxy resins. Here, the size of the region of sub-critical crack growth (termed the mirror zone) was found to increase with decreasing cyclic stress. Further, under certain conditions, the region of fast crack propagation was rough whereas in other cases it was completely smooth and featureless.

Fractographic studies of a silica-filled epoxy resin subjected to both short and long-term loading [9] highlighted three distinct zones on the fracture surface. The first, an area where the particles were found to be completely debonded from the neighbouring resin, was shown to represent the region of sub-critical crack growth. The second, a smooth featureless area, was found to represent the region of unstable crack acceleration. The third region was a rough three-dimensional zone, corresponding to the zone of crack propagation at the maximum attainable crack velocity, 820 m sec^{-1} at 23°C in this material.

Smith *et al.* [10] used thin sectioning techniques to examine the microstructural response of an unfilled and silica-filled epoxy resin to inelastic deformation.

Briefly, no damage was apparent at low temperatures and short test times whereas extensive localized shear yielding, particle–matrix debonding and micro-crack formation were in evidence at high temperatures and long test times.

In this investigation, the fracture behaviour of a silica-filled epoxy resin subjected to short-term tensile loading is examined. By integrating the information obtained from the volume and fracture surface observations, the mechanisms of failure initiation, propagation and fracture have been elucidated. Fundamental to this investigation is the characterization of the fracture surface morphology and the internal deformation damage as a function of the thermo-mechanical conditions of loading.

2. Experimental procedure

The material used in this investigation consisted of a hydantoin-based epoxy resin cured with an acid anhydride hardener. Silica flour with a mean particle size of $50\ \mu\text{m}$ was added, yielding a nominal particle volume fraction of 42%. Dumb-bell specimens of diameter 11.9 mm and effective gauge length 80 mm were cast in steel moulds. The curing process consisted of a gelation time of 4 h at 80°C followed by a 16 h post-cure at 130°C . This procedure resulted in a uniform distribution of particles and a glass transition temperature of approximately 125°C .

Tensile testing was conducted on a Zwick 1484 Universal testing machine at four temperatures: 23, 50, 85 and 105°C . The effect of loading rate on the initiation and development of damage was studied by using cross-head speeds of 0.1, 1.0, 10.0 and $50.0\ \text{mm min}^{-1}$.

The development of damage within the volume of the specimens was assessed by taking thin sections parallel to the direction of the applied load. The sectioning techniques are outlined in [10] and [11] and described in more detail by Smith [12]. Briefly, the specimen to be examined was cast into a block of epoxy resin and left to cure at room temperature. Once cured, the block was sectioned and polished parallel to the surface to be observed. This polished face was then glued to a non-birefringent plexiglass slide using an optically transparent adhesive. The majority of the block was then cut off the slide leaving a thin slice of material on the base slide. This was then ground and polished to give a section suitable for examination in transmitted light. The microscope was an Olympus BHSM compound microscope equipped with polarizers.

Two types of section were prepared, the first being approximately $80\ \mu\text{m}$ thick and viewed in bright-field transmitted light in order to identify any prevalent debonding and the second being $20\ \mu\text{m}$ thick was viewed in polarized light permitting the identification of localized shear yielding. The fracture surfaces of the failed specimens were examined using a low-power Olympus optical microscope and a Cambridge Instruments S100 scanning electron microscope.

A series of fracture toughness tests were conducted using single-edge notch specimens with dimensions $75\ \text{mm} \times 30\ \text{mm} \times 4\ \text{mm}$. Sharp pre-cracks of

nominal length 8 mm were introduced using a sharp razor blade.

3. Results and discussion

Short-term tensile tests on this silica-filled epoxy resin yielded a wide spectrum of differing fracture surfaces and varying degrees of volume damage. Initially, the variation of the fracture surface morphology as a function of both test rate and temperature will be considered. Following this, the variation of volume damage with test conditions will be assessed. Finally, the information gathered from these observations is brought together in order to identify the role of volume damage on the process of fracture in the filled epoxy.

3.1. Fracture surface characterization

A detailed examination of the failed specimens highlighted three distinct zones or regions on the fracture surfaces as shown schematically in Fig. 1. Failure usually initiated from some defect or large particle usually in a region of stress concentration, this being in most cases the parting line of the two mould halves. In the region surrounding the defect the particles were often debonded from the neighbouring matrix. Previous work [9] has shown that this area of extensive particle–matrix debonding represents the region of slow, sub-critical crack growth and that its extent and size depend strongly upon the prevailing thermo-mechanical test conditions at the moment of fracture. Consequently, this region is termed the sub-critical zone. Beyond this debonded area the crack begins to propagate unstably and produces a smooth, flat zone displaying few, if any, features. This smooth zone is then superceded by a much rougher three-dimensional zone in which the crack has clearly bifurcated producing multiple localized fracture surfaces.

The variation of tensile strength with temperature and test rate is shown in Fig. 2. This curve is not intended to be a thorough investigation of the variation of tensile strength with thermo-mechanical loading conditions, because only one test has been undertaken at each condition. Instead, the curve is shown in order to supplement the information

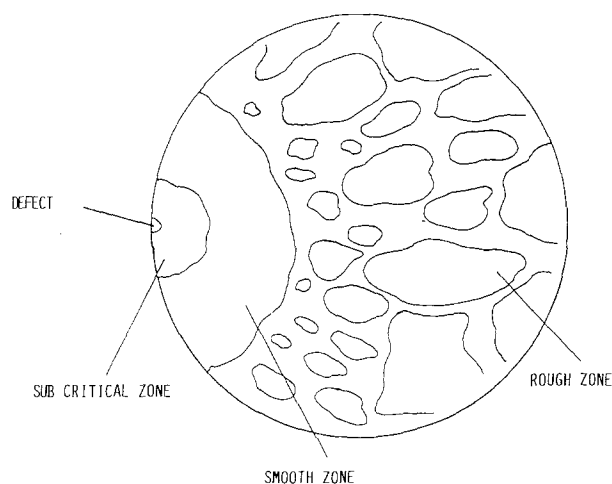


Figure 1 Schematic representation of the fracture surface of the silica-filled epoxy.

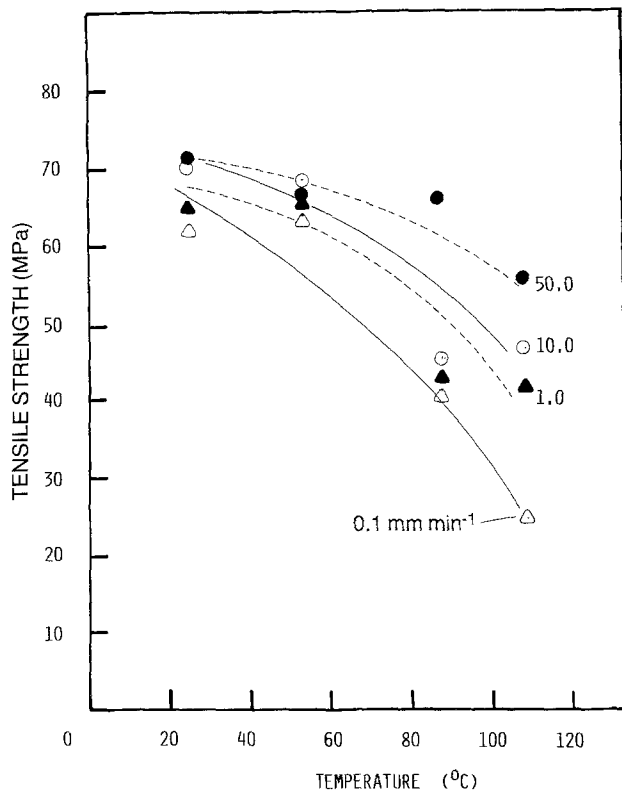


Figure 2 The variation of tensile strength with test temperature and cross-head speed for the silica-filled epoxy. (●) 50, (○) 10, (▲) 1, (△) 0.1 mm min⁻¹.

presented in the following sections detailing the fracture surface characteristics and the development of volume damage. The increase in tensile strength with decreasing temperature and increasing loading rate are indicative of the typical rate-temperature equivalence found in most polymers. At the highest temperature and lowest cross-head speed the tensile strength of the material is only about one-third of its value at room temperature.

The following sections consider the formation of the various zones apparent on the fracture surfaces of this filled epoxy in more detail and assesses the influence of the test rate and temperature on their relative size and consequence.

3.2. The sub-critical zone

As previously stated, the sub-critical zone is generally located near some form of initial defect and represents

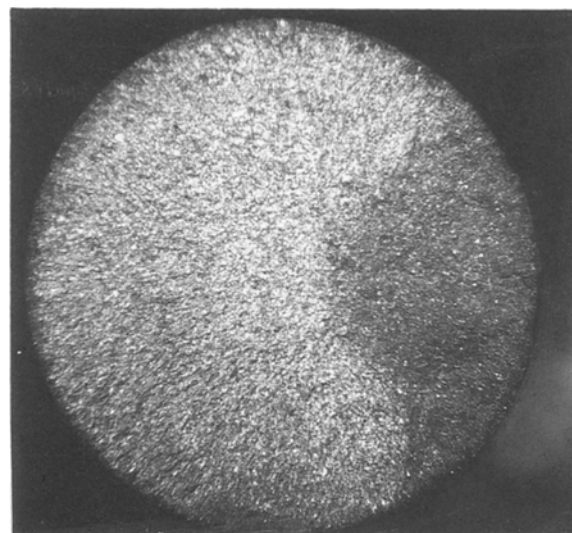


Figure 3 Gold-coated fracture surface of a specimen tested at 0.1 mm min⁻¹ and 105°C showing the sub-critical zone.

a region in which the particles are completely debonded from the neighbouring matrix. Fig. 3 shows the fracture surface of a specimen tested at 0.1 mm min⁻¹ and 105°C. Here, the surface has been coated with a thin layer of gold in order to improve the level of contrast between the sub-critical region and the remaining fracture surface. In this specimen the crack has grown approximately 5 mm across the fracture surface, this representing the largest sub-critical zone size observed in this programme of tests. Upon reaching this size the crack became unstable and accelerated rapidly precipitating a rapid brittle fracture.

Fig. 4 shows two sub-critical zones taken from specimens tested at 50 and 105°C and 0.1 mm min⁻¹. It is immediately apparent that virtually all of the particles visible in each photo are debonded. A closer examination of the photos indicates that the gap between the particles and the neighbouring matrix is greater at the higher temperature suggesting that more plastic deformation of the matrix has occurred during the slow crack growth at this condition. Previous work [9], using the double-torsion test geometry, substantiates the belief that this debonding process occurs only at very low crack velocities and has shown that the debonding threshold velocity increases with increasing test temperature. This is shown clearly in Fig. 5 where particle-matrix debonding was observed

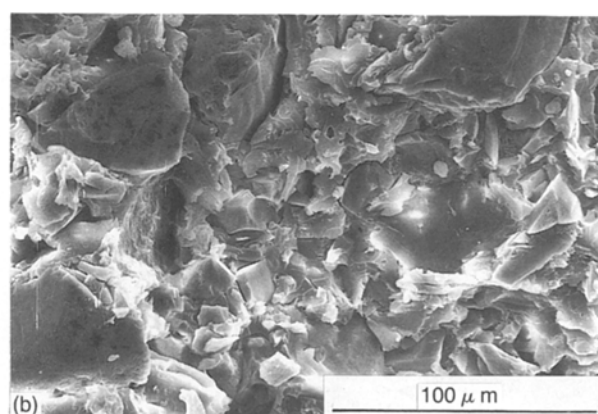
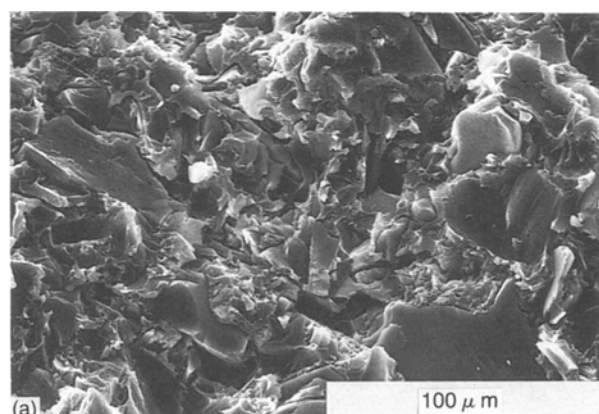


Figure 4 Scanning electron micrographs of the sub-critical zone; (a) 0.1 mm min⁻¹, 50°C, (b) 0.1 mm min⁻¹, 105°C.

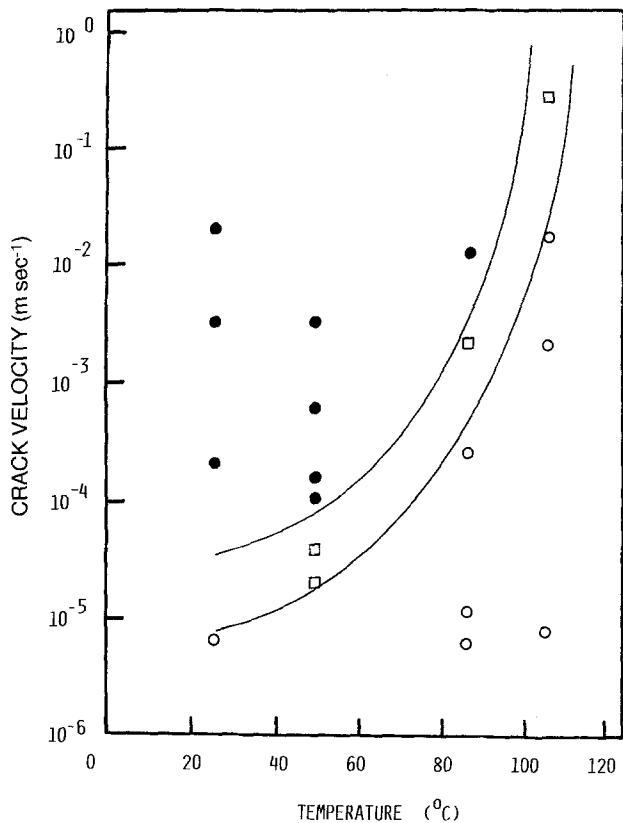


Figure 5 The variation of the debonding threshold velocity with temperature for double-torsion specimens. (●) Fully bonded particles, (□) partial debonding, (○) fully debonded. From [9].

only at velocities below $10^{-5} \text{ m sec}^{-1}$ at 23°C but at all velocities up to 0.5 m sec^{-1} at 105°C . It is believed that the debonding process during crack propagation is initiated by the plastic zone extending in front of the crack tip. Essentially, the large strains generated by the localized deformation in front of the crack exceeds the failure strain of the particle-matrix interface thereby precipitating localized debonding.

In this work, the size of the sub-critical zone was found to depend upon the test rate and temperature. The variation of the size of this zone with temperature for a fixed cross-head speed of 0.1 mm min^{-1} is shown in Fig. 6. At the lowest temperature only a very small number of particles around the initial defect were

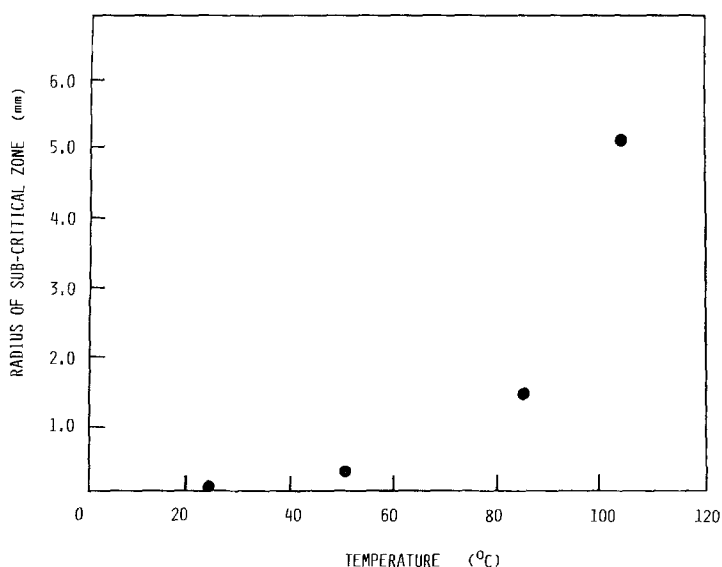


Figure 6 The variation of the size of the sub-critical zone with temperature for a cross-head speed of 0.1 mm min^{-1} .

debonded and it proved difficult to measure the size of this zone with any accuracy. Conversely, at the highest temperature the subcritical zone occupied a large percentage of the fracture surface and was clearly visible to the naked eye.

Similar trends were noted in the variation of the size of the sub-critical region with cross-head speed for a given temperature. Fig. 7 shows such a curve for the results obtained at 105°C . The complete array of curves for the various cross-head rates and test temperatures examined here are presented in Fig. 8. At the highest rates and lowest temperatures the number of debonded particles around the defect was quite small and difficult to quantify. Indeed, many of the specimens tested at 23°C showed no evidence of particle-matrix debonding when viewed either optically or with the scanning electron microscope. In these cases, it appears that one single debonding event proved sufficient to precipitate an instability and therefore rapid specimen failure. The evidence presented in Fig. 8 tends to support the view that the debonding process is related to the yielding characteristics of the material, i.e. fracture surface debonding is more prominent when the yield stress of the material is low, that is, at low test rates and high test temperatures.

In order to assess the influence of damage on the fracture toughness of this material a number of single-edge notch tests were undertaken on specimens of dimensions $75 \text{ mm} \times 30 \text{ mm} \times 4 \text{ mm}$. A total of four specimens were tested at each condition. The resulting variation of K_{Ic} with temperature for a cross-head speed of 1.0 mm min^{-1} is shown in Fig. 9. Examination of the curve indicates that the toughness of the material remains approximately constant for all of the temperatures examined here. A subsequent examination of these specimens failed to highlight any particle-matrix debonding on these specimens. When viewed in transmitted light, the sections removed from these specimens failed to show any significant yielding process at the crack tip.

It is suggested, therefore, that at this cross-head speed the constraining influence of the silica particles coupled with the relatively high yield stresses under these conditions do not permit a significant increase in

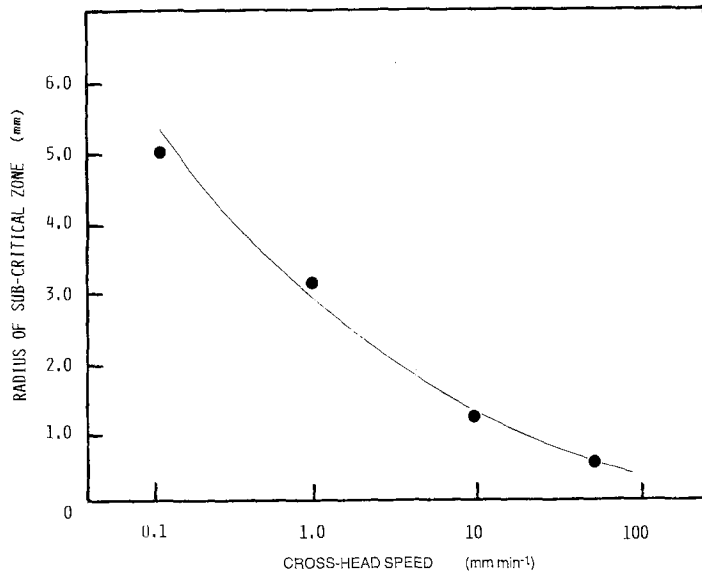


Figure 7 The variation of the size of the sub-critical zone with cross-head speed at temperature 105°C.

the size of the crack tip plastic zone with increasing test temperature. As a consequence, there is no significant blunting or softening at the crack tip and the fracture toughness does not vary with increasing test temperature.

The variation of K_{Ic} with cross-head speed at 105°C is presented in Fig. 10. Here, decreasing the cross-head speed between 50 and 1.0 mm min⁻¹ did not result in any significant increase in the fracture toughness. Once again, none of these specimens exhibited any form of particle-matrix debonding or localized shear yielding on the fracture surface or in the volume. However, a significant decrease in fracture toughness was noted in the specimens tested at 0.1 mm min⁻¹. Here, a large region of debonded particles was observed in front of the initial pre-crack suggesting that the crack had propagated in a sub-critical manner over a distance of several millimetres. When corrected for this extension in initial crack length the value of K_{Ic} was still considerably below that measured at 1.0 mm min⁻¹. When sectioned and viewed under polarized light, a large process zone measuring over 1 mm long consisting of debonded particles was observed in front of the crack tip, Fig. 11. This suggests that the debonding process ahead of the crack degrades the

toughness of the material and may result in the premature failure of the specimen. In this case, instead of inducing a toughening mechanism, the particles provoke isolated fractures in a zone in front of the main crack and therefore reduce the materials toughness.

From these results it appears that a moderately sized process zone in front of the crack tip is neither advantageous nor detrimental; however, a large process zone (i.e. many particle diameters in size) is disadvantageous because it results in the formation of small cracks in front of the main crack. This is represented in schematic form in Fig. 12. Similar conclusions were drawn by Evans *et al.* [13] following an analytical analysis of the toughness characteristics of particulate-filled polymers. Here it is suggested that debonding represents a loss in section and that the simplest expression for the toughness degradation, J^d , is given by

$$J^d = J^m(1 - v)$$

where J^m is the reference fracture resistance of the material and v the volume fraction of particles.

The variation of the tensile failure stress with sub-critical zone size for the specimens tested at 105°C, Fig. 13, indicates, as expected, that the failure stress

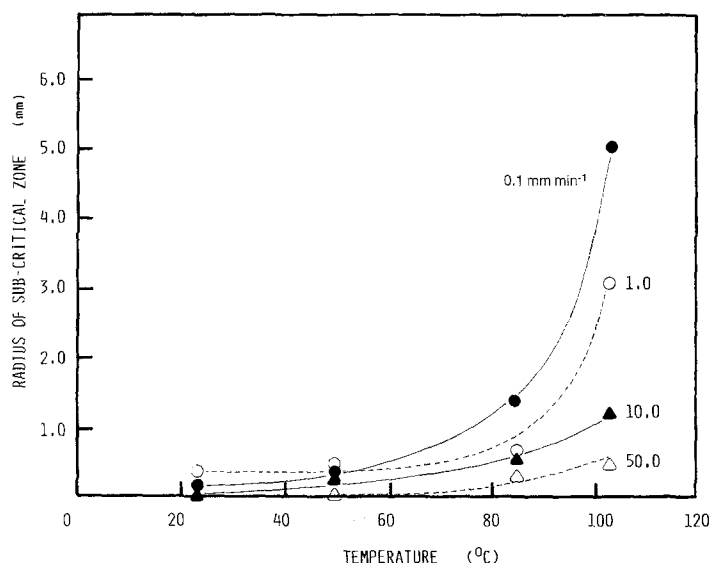


Figure 8 The variation of the size of the sub-critical zone with both temperature and cross-head speed.

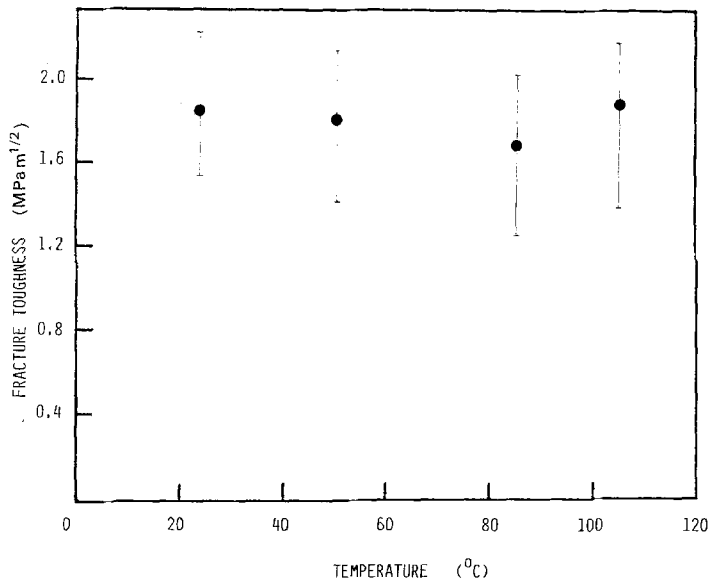


Figure 9 The variation of K_{Ic} with temperature for a cross-head speed of 1.0 mm min^{-1} for this silica-filled epoxy.

decreases as the sub-critical zone size increases. Previous work on this material [9] has shown that it is possible to relate the failure stress of the specimen to the sub-critical zone size via a fracture mechanics analysis. No such attempt was made here, however, since many experimental parameters have been changed from test to test.

3.3. The smooth zone

The region surrounding the sub-critical zone, termed the smooth zone, exhibits a flat, featureless appearance. In this region the fracture surface is essentially matrix dominated and the particles remain well bonded to the matrix as shown in the scanning electron micrographs presented in Fig. 14. The size of this zone varies with both loading rate and temperature as shown by the fracture surfaces presented in Figs 15 and 16. At the lowest temperatures and highest rates the smooth zone is quite small, measuring only several millimetres in size. Conversely, at the highest temperature and lowest rate the fracture surface is completely smooth and exhibits only a sub-critical zone and a smooth zone, Fig. 15d. The information presented in these two figures was quantified by measuring the size of the smooth zone as a function of temperature and rate.

The results of this procedure are presented in graphical form in Fig. 17. The trends in the data are similar to those observed for the sub-critical zone, that is, its size increases with increasing temperature and decreasing rate.

The significance of the smooth zone has previously been assessed by conducting tests on a series of single-edge notch specimens [9]. Here, using the graphite gauge technique in order to measure the variation of crack velocity with time it was shown that the smooth zone corresponds to the area over which the unstable crack is accelerating up to the material's limiting velocity (820 m sec^{-1} at 23°C in this material). This is shown clearly in Fig. 18a where the variation of crack velocity along the fracture surface of a single-edge notch specimen is presented. If the crack does not reach the material's limiting velocity the resulting fracture surface is completely smooth and exhibits no evidence of crack bifurcation, Fig. 18b. Consequently, it can be concluded that in all cases except the test at 105°C and 0.1 mm min^{-1} the crack reached the limiting velocity during the phase of unstable rupture.

The explanation for the smooth appearance of this zone is as follows. When the crack becomes unstable and begins to accelerate rapidly the elastic energy

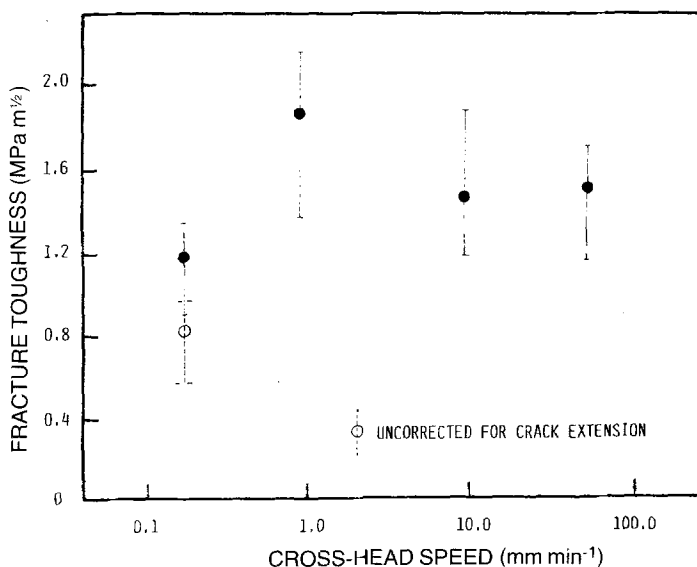


Figure 10 The variation of K_{Ic} with cross-head speed at 105°C .

stored within the specimen is dissipated by accelerating the crack. Any excess stored elastic energy is dissipated by simply further accelerating the crack. Once the limiting velocity has been reached it is no longer possible to continue accelerating the crack and another energy-dissipating mechanism must be used, i.e. crack bifurcation.

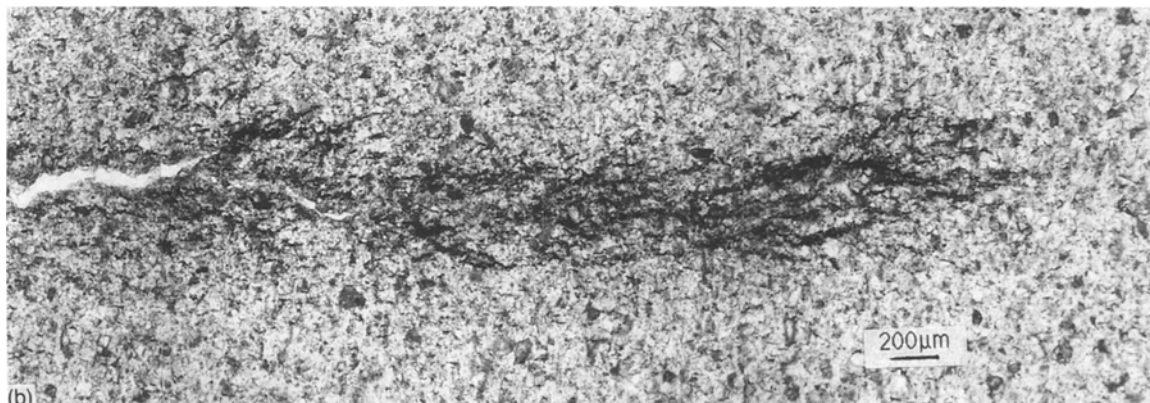
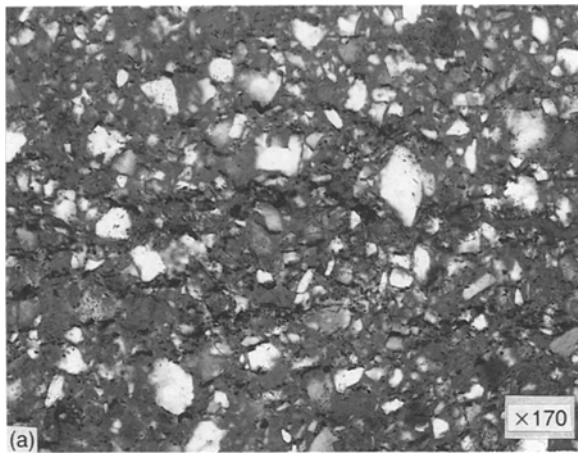
Similar zones have been observed on fractured glass rods [14] and glass fibres [15]. Many workers have subsequently attempted to relate the size of this zone, M_r , to the failure stress, σ_f , using the fracture mechanics-type relationship

$$\sigma_f M_r^{0.5} = \text{constant}$$

Here, such an analysis did not yield any unique form of relationship between these two parameters as shown in Fig. 19. Indeed, it is not fully clear why such a relationship should hold, because the stress within the specimen falls rapidly once the crack begins to propagate [16] and is therefore considerably less than its initial value once the crack has reached the end of the smooth zone. Similar fracture tests on a large number of single-edge notch specimens again failed to show any distinct relationship between these two parameters. We believe that the size of this zone is related to the amount of elastic energy available to accelerate the crack at the moment of instability. Indeed, previous work has shown that there exists a reasonable relationship between the energy available at rupture and the size of this zone [9].

3.4. The rough zone

The rough region exhibits a strong three-dimensional



appearance, this being associated with extensive branching of the principal crack. In the previous section it was shown that the unstably propagating crack has reached its limiting velocity in the rough region, this being approximately 820 m sec^{-1} at 23°C . This limiting velocity is temperature dependent, however, as shown in Fig. 20. Here, the maximum velocity attainable at 105°C is approximately 750 m sec^{-1} , this reduction probably being due to the reduction in elastic modulus and, therefore, in sonic speed at this temperature.

The scanning electron micrographs taken in this region indicated that the fracture surface was again matrix dominated exhibiting no evidence of particle-matrix debonding, Fig. 21.

Both the size and the roughness of this zone varied with rate and temperature as shown in Figs 15 and 16. At the lowest temperatures and highest rates substantial amounts of crack branching were in evidence and the fracture surface exhibited a very uneven appearance. At the higher temperatures and lower rates the fracture surfaces were noticeably less rough. Indeed, at 105°C and 0.1 mm min^{-1} the fracture surface was completely smooth suggesting that the crack had not reached the limiting velocity.

It is believed that the roughness of this zone is related to the amount of stored elastic energy available at the moment of unstable fracture. The evidence presented in Figs 15 and 16 tends to support this view because the fracture surfaces were rougher for conditions when the area under the stress-strain curve was greatest, that is, at the lowest temperatures and highest rates. The trends apparent in Figs 15 and 16 were quantified by tracing the areas of crack bifurcation with transparent paper and calculating the percentage of the rough zone showing crack branching. The results of this analysis are presented in Fig. 22. Although somewhat laborious, this procedure does appear to support the visual evidence apparent in the photographs of the fracture surfaces shown previously in Figs 15 and 16.

Having successfully explained and quantified the features evident on the fracture surfaces of this silica-

Figure 11 The development of damage in front of the crack tip in a single-edge notch specimen tested at 0.1 mm min^{-1} and 105°C : (a) thin section (thickness $50 \mu\text{m}$) showing debonding and matrix microcracks at the crack tip; (b) thin section (thickness $100 \mu\text{m}$) showing the entire damage zone ahead of the crack.

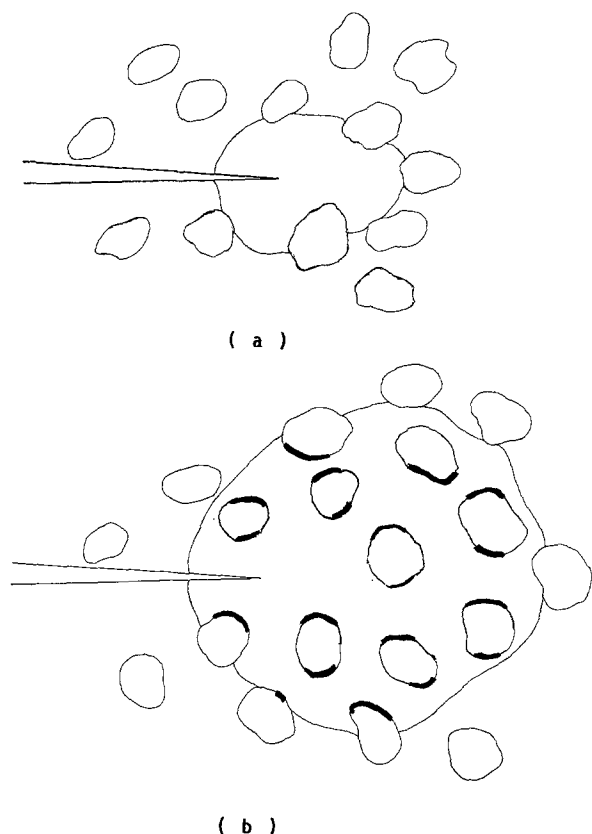


Figure 12 Schematic representations of the process zone in front of the crack tip: (a) usual case where the process zone size is of the same order as the inter-particle size; (b) detrimental case because the process zone encompasses a large number of particles in front of the crack tip.

filled epoxy resin, thin sections were prepared parallel to the direction of the applied load in order to assess the initiation and development of damage within the volume of this material. The findings of this analysis will be discussed in the following sections.

3.5. Volume damage studies

3.5.1. Macroscopic damage

A macroscopic investigation of the failed specimens indicated that many of those tested at the highest temperatures and lowest rates exhibited some form of discoloration or stress whitening. Such whitening usually took the form of a milky band running along the moulding line as shown in Fig. 23. No such whitening was observed at 23, 50 and 85°C, except at

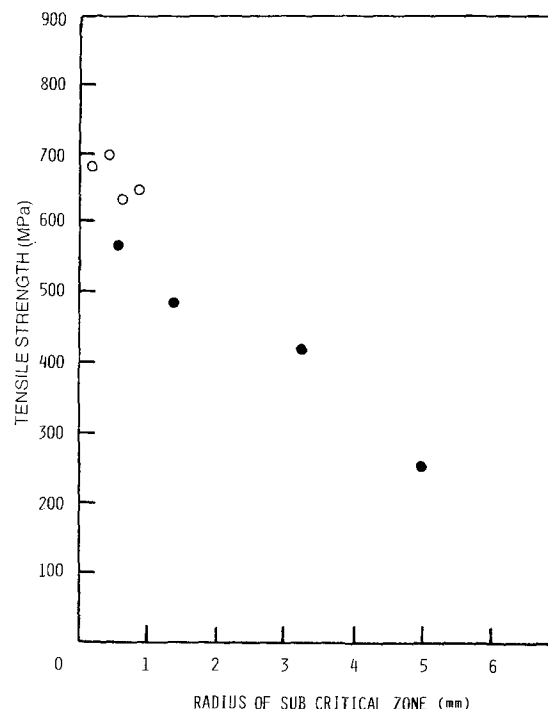


Figure 13 The variation of tensile failure stress with the size of the subcritical zone. (○) 50°C, (●) 105°C.

85°C and the slowest rate (0.1 mm min^{-1}), where it was localized at several cracks visible at the mould parting line. A previous investigation into the processes of damage development in this material [10] has shown that such stress whitening is due to particle-matrix debonding within the volume.

3.5.2. Microscopic damage

In order to observe the mechanisms of internal damage development within this material, thin sections were taken from many of the fractured specimens. These sections were generally taken parallel to the direction of applied load, then ground and polished and examined in transmitted bright field and polarized light.

An extensive examination of these sections permitted a detailed analysis of the mechanisms of inelastic deformation and fracture occurring within the material. Essentially, four mechanisms were identified within the specimens, these being localized shear yielding, particle-matrix debonding, matrix micro-cracking

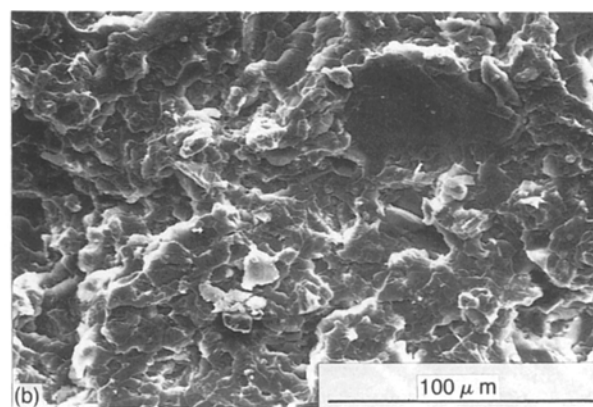
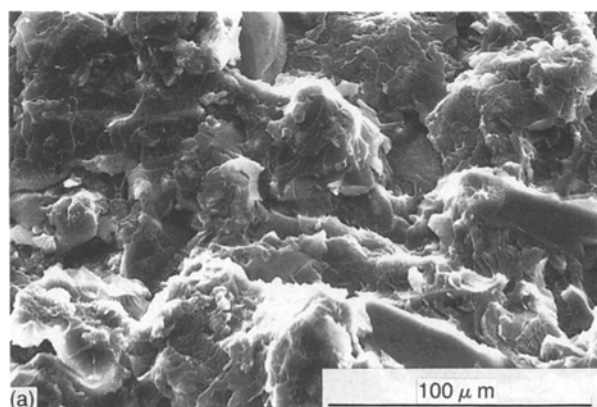


Figure 14 Scanning electron micrographs of the smooth zone in specimens tested at (a) 0.1 mm min^{-1} , 50°C, and (b) 0.1 mm min^{-1} , 105°C.

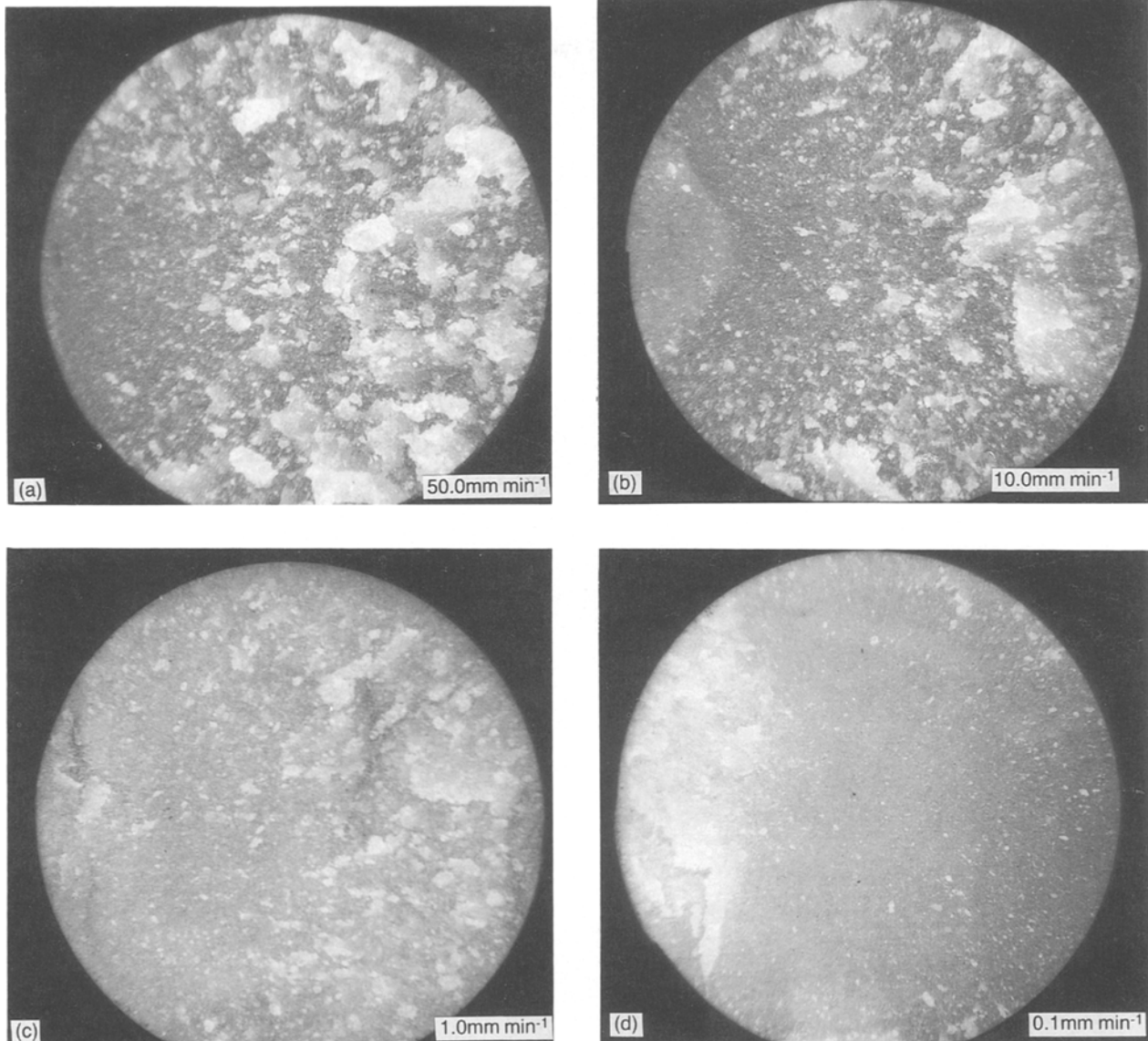


Figure 15 Photographs of the fracture surfaces of specimens tested at 105°C: (a) 50 mm min⁻¹; (b) 10 mm min⁻¹; (c) 1.0 mm min⁻¹; (d) 0.1 mm min⁻¹.

and particle fracture. The latter, particle fracture, was observed only occasionally, its extent being considerably less than observed in compression-loaded samples [10].

The following section details the effect of varying the test temperature on the initiation and development of such damage within the volume of these specimens.

3.5.3. The effect of temperature on damage development

At 23 and 50°C there was no evidence of any form of inelastic deformation or damage within the volume of the material. Under these conditions failure is most likely due to the debonding of a single particle. Here, in the absence of any localized plastic deformation the stress concentration associated with one such debonding event was probably sufficient to precipitate an instability and a subsequent rapid brittle fracture.

At 85°C a number of isolated debonding events were observed within the volume of the specimen tested at 0.1 mm min⁻¹, Fig. 24. These debonds did not appear to occur preferentially in one zone but tended to occur at the largest particles within the

volume of the material. At the highest temperature, 105°C, extensive damage was apparent within the regions of extensive stress whitening, Fig. 25. A closer examination of the sections indicated that almost all of the particles in the stress-whitened zones were debonded and that the material appeared to be completely degraded. Further, under these conditions, many of the debonds started to coalesce forming a complex array of micro-cracks throughout the damaged volume. When examined under polarized light, a network of fine shear bands around the particles was observed as shown in Fig. 26. In areas away from such extensive stress-whitening, debonding was sparse and sometimes not in evidence at all.

The damage evident in the thin sections was quantified by counting the number of debonded particles in a 2 mm square region taken from the most damaged area of each specimen. Fig. 27 shows the variation of the number of debonds as a function of the test temperature for the tests undertaken at 0.1 mm min⁻¹. The onset of debonding at 85°C was clearly detected by this technique as well as the rapid rise in the number of debonding events between 85 and 105°C.

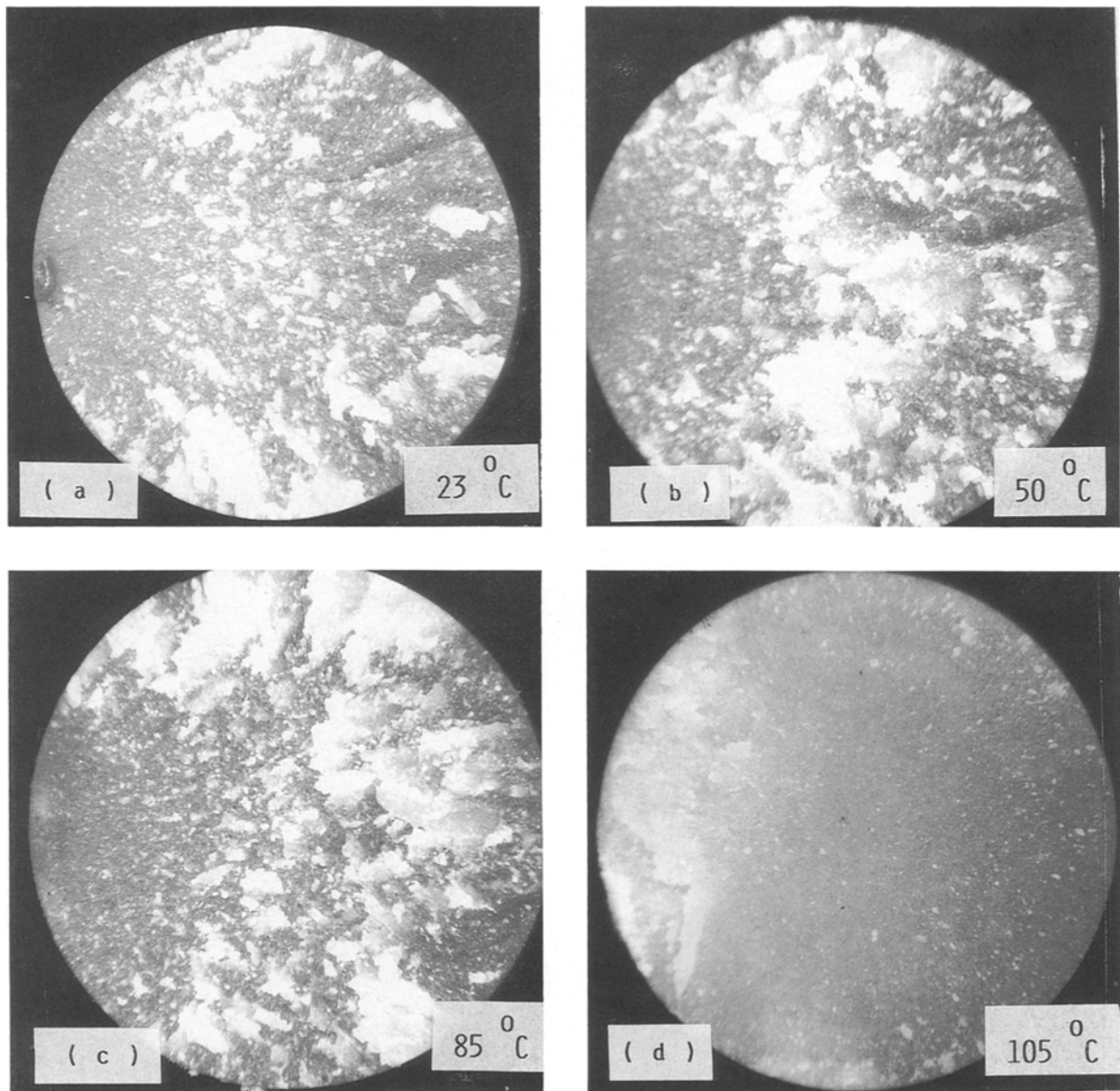


Figure 16 Photographs of the fracture surfaces of specimens tested at 0.1 mm min^{-1} : (a) 23°C ; (b) 50°C ; (c) 85°C ; (d) 105°C .

3.5.4. The effect of test rate on damage development

The influence of test rate on damage development was most marked at 105°C . At 50 mm min^{-1} at this temperature, volume damage was limited to a few isolated

debonded particles distributed randomly throughout the volume of the material. A limited number of shear bands were identified at 10 mm min^{-1} accompanied by increased isolated debonding. By 1.0 mm min^{-1} shear bands were clearly evident, many of the particles were

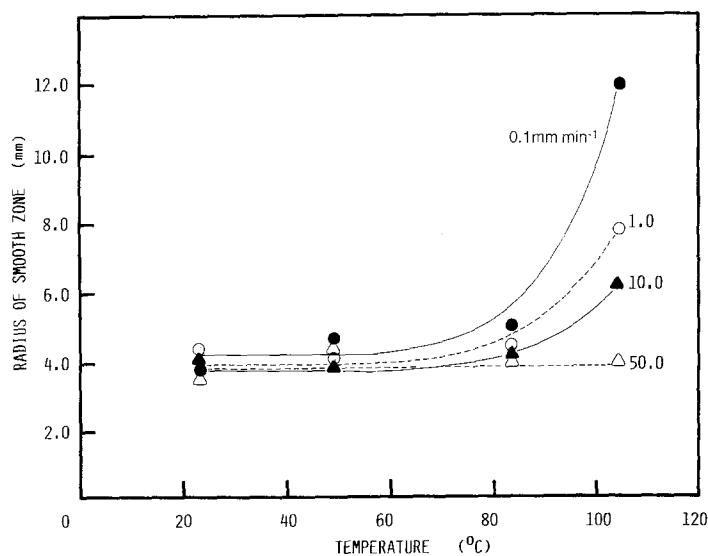


Figure 17 The variation of the size of the smooth zone as a function of test temperature and rate.

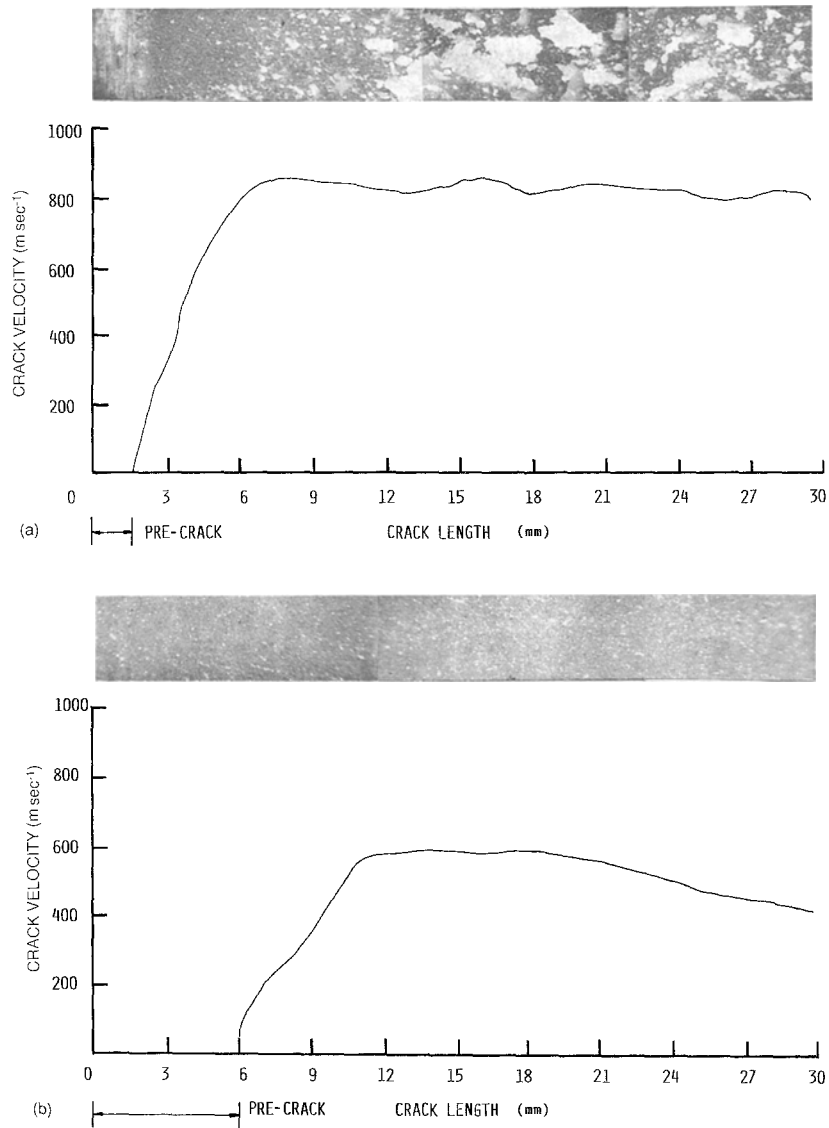


Figure 18 The variation of crack velocity along the fracture surfaces of two single-edge notch specimens tested at 23°C; (a) the crack reaches the material's limiting velocity; (b) the crack does not reach this limiting velocity.

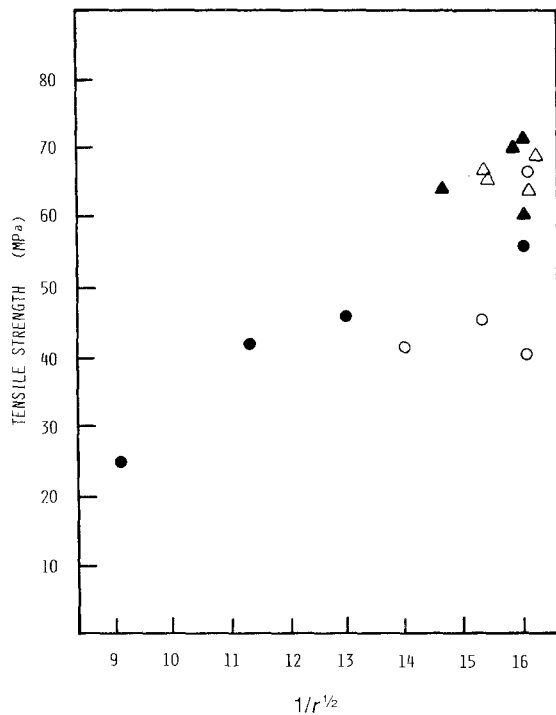


Figure 19 The variation of tensile strength with the inverse square root of the smooth zone radius, r . (Δ) 23°C, (\blacktriangle) 50°C, (\circ) 85°C, (\bullet) 105°C.

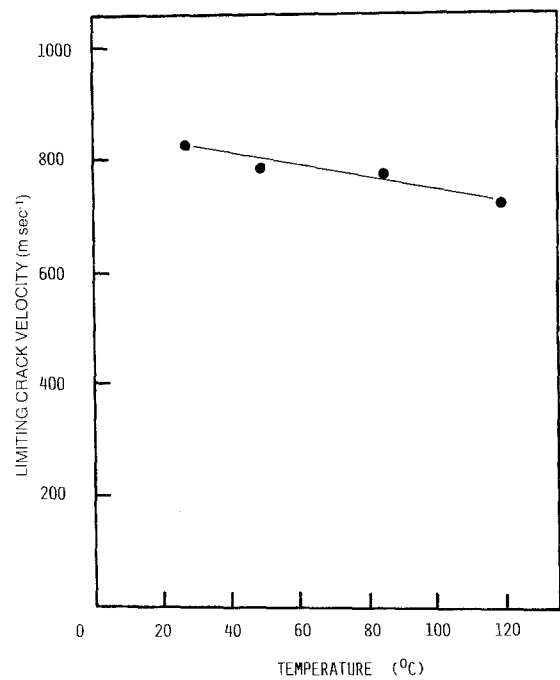


Figure 20 The variation of the maximum attainable crack velocity with test temperature. Data obtained from single-edge notch tests.

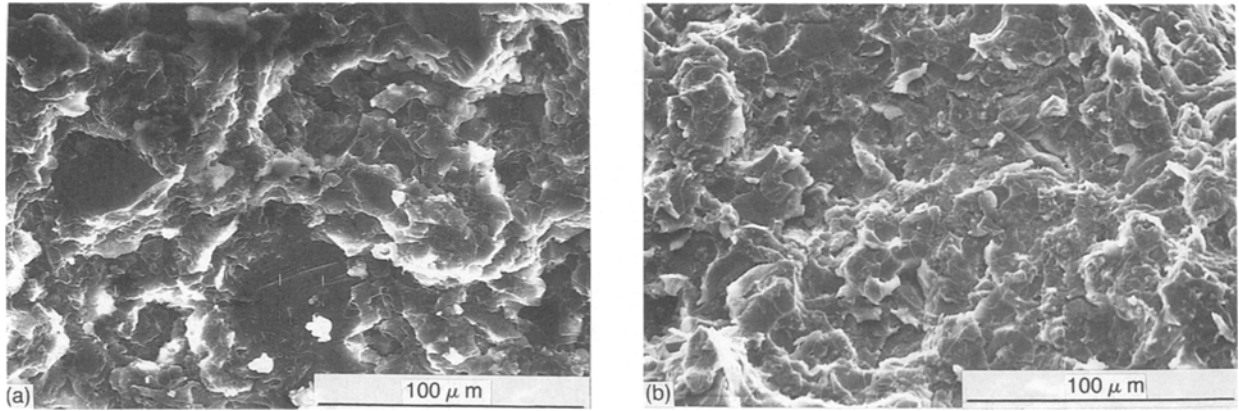


Figure 21 Scanning electron micrographs of the rough zone in specimens tested at (a) 0.1 mm min^{-1} , 50°C ; (b) 10.0 mm min^{-1} , 105°C .

debonded and evidence of micro-cracking between particles was apparent. The damage at 0.1 mm min^{-1} 105°C was extensive with debonding, shear bands and micro-cracking as discussed above. Here, almost all of the particles were debonded and a large number of micro-cracks were visible throughout the volume of the specimen. As before, the information obtained from the thin sections was quantified by counting the number of debonds in a 2 mm square zone exhibiting the most damage. The variation of the number of debonded particles with cross-head speed at 105°C is presented in Fig. 28. Here, the number of debonded particles appears to drop linearly with increasing strain rate on this semi-log plot.

3.6. Summary of the fracture processes and their dependence on temperature and rate

The information gathered from these tests provides a greater insight into the process of inelastic deformation and fracture in rigid particulate-filled epoxies. It is now apparent that tension-induced damage begins when the local strain within the material exceeds the failure strain of the interface. At the faster rates at 23 and 50°C one such debonding event generally proved sufficient to precipitate complete specimen failure. Conversely, at 105°C 0.1 mm min^{-1}

damage was extensive with stress-whitened zones in which almost every particle was debonded from the neighbouring matrix. If the local yield stress of the material is sufficiently low, the free surface created by the debonding process may encourage localized shear yielding within the matrix. If these voids then begin to propagate away from the particle the local constraint given to the matrix is reduced and the material can relax relieving the shear bands. Consequently, in the regions of extensive micro-cracking it often proved difficult to highlight any form of localized inelastic deformation.

The results of these damage studies are summarized in the damage mechanism map presented in Fig. 29. Briefly, localized shear yielding was observed only at the three slowest rates at 105°C . Debonding within the volume of the material was observed only at the lower cross-head speeds at 85°C and at all rates at 105°C . Micro-cracking was observed essentially only at the lowest rates at 105°C .

The information gathered from these tests confirms the general observation that the process of fracture may change with rate and temperature. In our case, three possible scenarios for failure have been identified, these being rapid brittle fracture due to a single debonding event, fracture due to the development of localized damage in the process zone at the tip of the

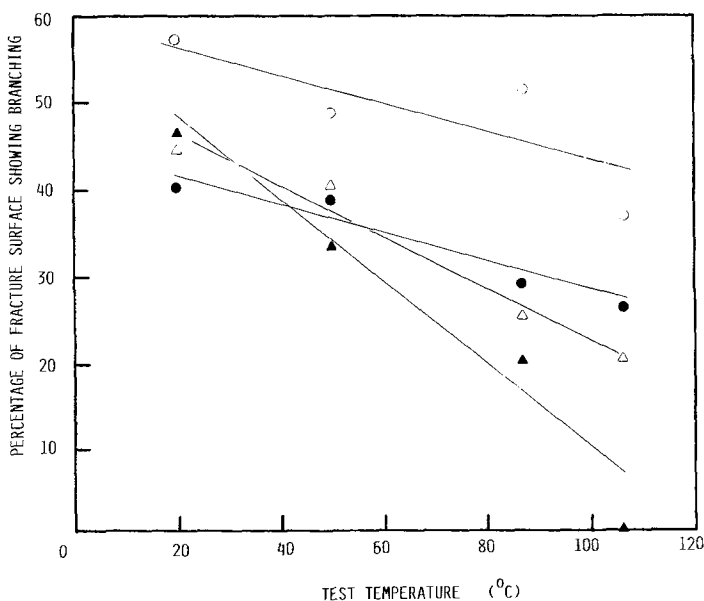


Figure 22 The variation of the percentage area of the rough zone showing crack bifurcation. (○) 50 , (●) 10 , (△) 1.0 , (▲) 0.1 mm min^{-1} .

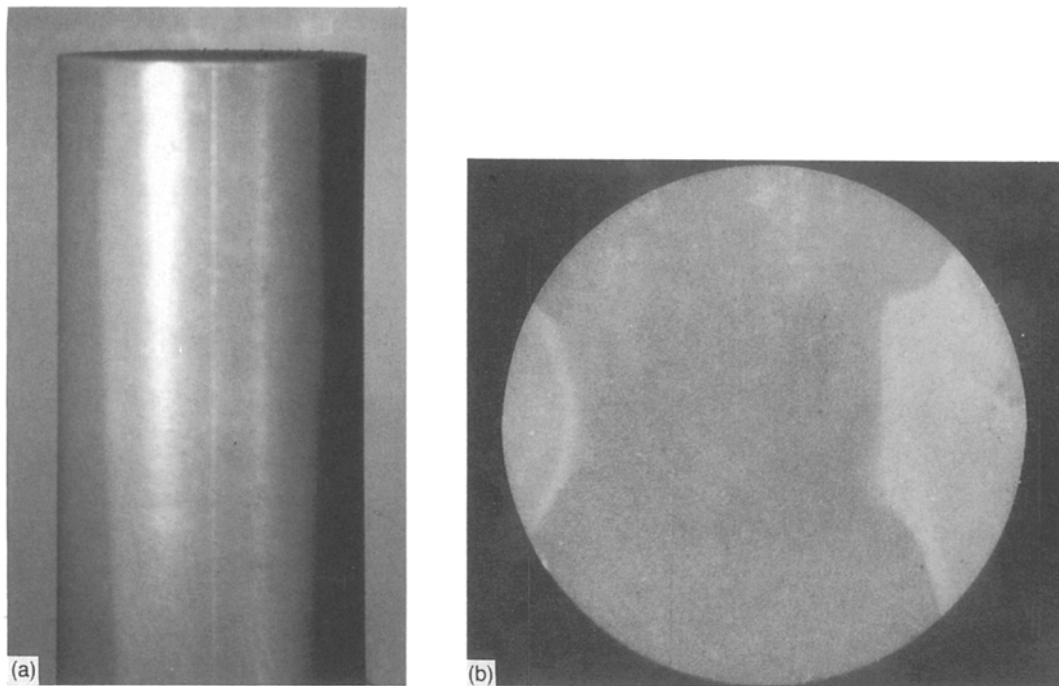


Figure 23 Photographs of a specimen tested at 0.1 mm min^{-1} , 105°C , showing the stress whitening (a) on the exterior of the specimen, and (b) through the cross-section just below the fracture surface.

crack and fracture associated with the presence of extensive damage within the volume of the material. The following sections will summarize each of these failure processes in more detail.

3.6.1. Rapid brittle fracture

Rapid brittle fracture occurs at low temperatures in the absence of significant plastic deformation. Here, the debonding of a single particle produces a stress concentration sufficient to initiate an instability and instantaneous specimen failure. In this case no damage or shear yielding is evident in the volume.

3.6.2. Crack propagation by debonding

When the process zone at the crack tip encompasses several particles, debonding may occur as a result of the locally high strains at the particle–matrix interface. As a result, the crack tends to propagate by the generation of small debonds at its tip. This is shown in schematic form in Fig. 30a. As a consequence, the

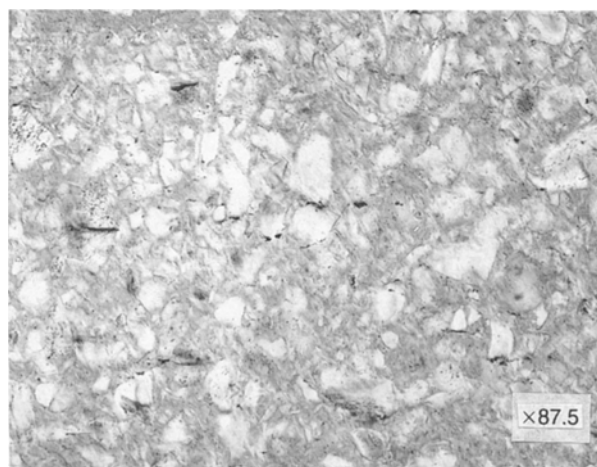


Figure 24 Limited particle–matrix debonding in a specimen tested at 0.1 mm min^{-1} , 85°C , $\times 125$.

resulting sub-critical zone tends to be quite smooth and perpendicular to the applied load. This type of behaviour was observed in the specimens tested at the lower cross-head speeds at temperatures of 85°C and below as well as those tested at the higher cross-head speeds at 105°C .

3.6.3. Crack propagation by coalescence of debonding

At the higher temperatures and the lower rates extensive damage taking the form of debonding and micro-

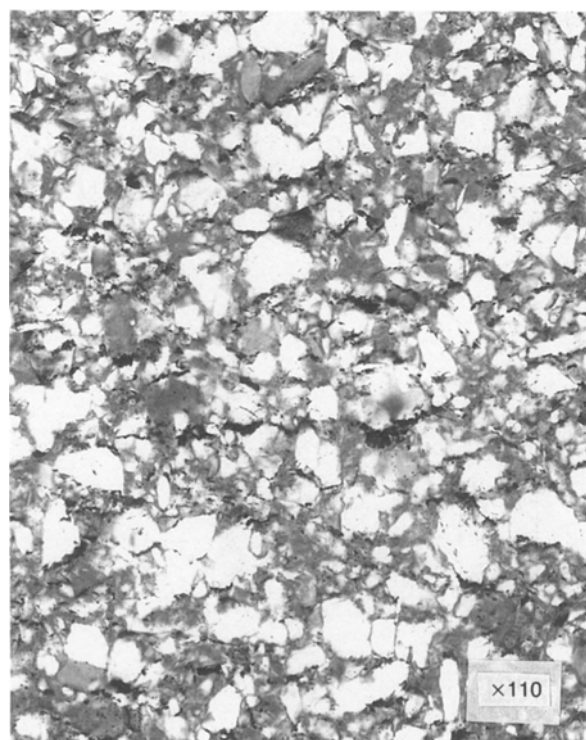


Figure 25 Damage in a specimen tested at 0.1 mm min^{-1} , 105°C , $\times 125$.

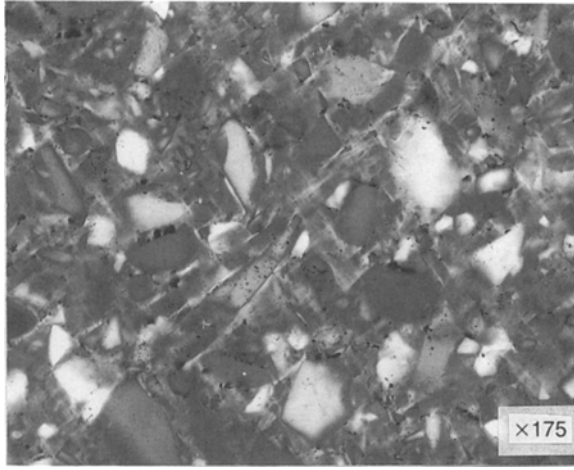


Figure 26 Localized shear yielding in a specimen tested at 0.1 mm min^{-1} , 105°C , $\times 250$.

cracking was generated within the volume of the material prior and during sub-critical crack growth. Such damage will clearly degrade the material and influence the process of slow stable crack growth. When examined in detail it was found that the sub-critical zone in this material was very uneven suggesting that the crack had propagated out of plane. This is clearly shown in Fig. 31 where the profiles of two fractures surfaces have been reproduced from the photographs taken from the corresponding thin sections.

This phenomenon was explained by considering the interaction of the sub-critical crack with the extensive volume damage generated within certain parts of the material during the course of testing. As previously stated, the development of damage within specimens tested at high temperatures and low rates is continuous and occurs within the volume of the material. Once a crack begins to grow, its propagation will obviously be influenced by the existing damage. Micro-cracks and debonded particles exist within the vicinity of the principal crack cause the crack to deviate out of plane and follow a path determined by the presence of such damage. This process is depicted in Fig. 30b. The resulting sub-critical zone exhibits a

much rougher appearance than observed in the specimens in which no significant amounts of volume damage was generated.

The stress-whitening of the specimens tested at the highest temperatures is caused by particle-matrix debonding within the volume of the material. Such material is degraded internally and offers considerably reduced mechanical properties. Tests to assess the effect of stress whitening on the load-carrying capability of this material have suggested that such damage may reduce its flexural strength by up to 25% [17]. Further, such damage is not recoverable by upon heating to the glass transition temperature [10].

4. Conclusions

A fractographic analysis of the failed specimens highlighted three distinct regions on the fracture surfaces. Around the defect many of the particles were often debonded as a result of the sub-critical growth of the crack. The size of this zone varies considerably with temperature and rate. At the onset of instability, the fracture surface becomes very smooth and the particles remain well bonded to the matrix. This smooth zone corresponds to the region of unstable crack acceleration. Beyond this zone the fracture surface becomes very rough exhibiting extensive crack bifurcation. Here the crack is propagating at the limiting velocity and much energy is being dissipated in creating multiple fracture surfaces. Once again, the physical appearance of this zone depends upon the thermo-mechanical testing conditions.

The effect of test temperature and loading rate on the initiation and development of damage within a silica-filled epoxy resin has been studied. Three different types of inelastic and fracture processes within the volume of the material have been identified, these being, localized shear yielding, particle-matrix debonding and micro-cracking. At low temperatures and high rates one single debond is usually sufficient to precipitate a catastrophic failure. At intermediate temperatures and low cross-head speeds the cracks propagated by debonding particles in a small zone in front of the crack tip. At the highest temperature the

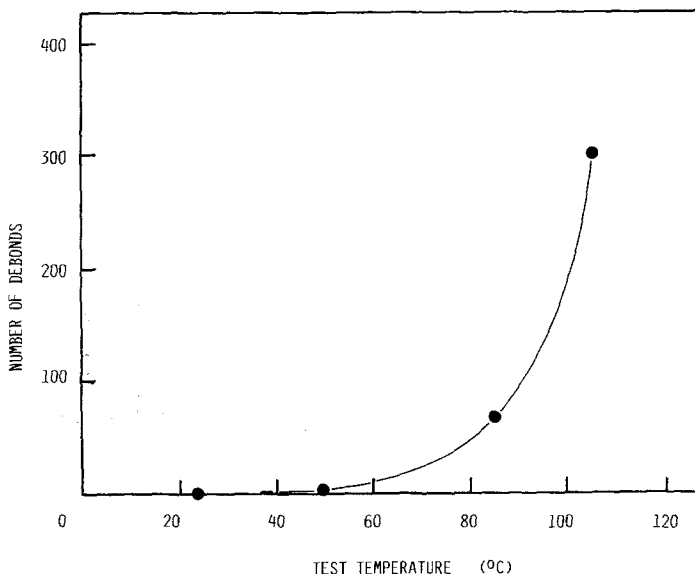


Figure 27 The variation of the number of debond events with temperature for a cross-head speed of 0.1 mm min^{-1} .

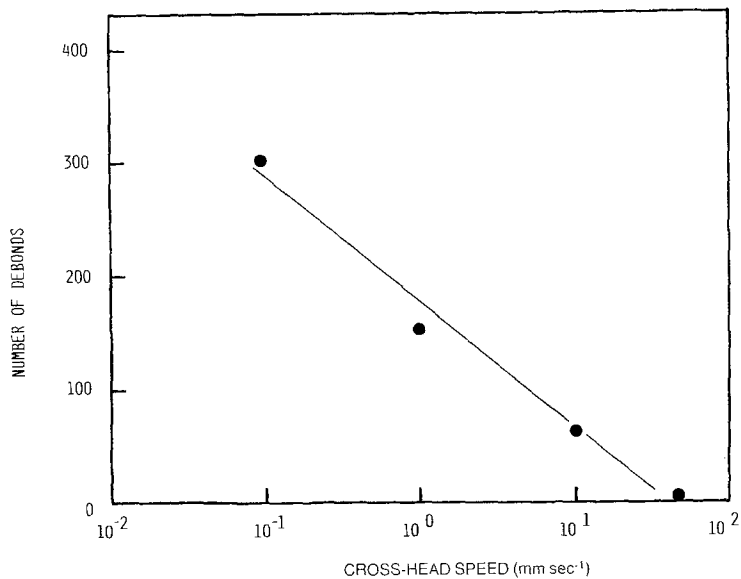


Figure 28 The variation of the number of debond events with cross-head speed for a temperature 105°C.

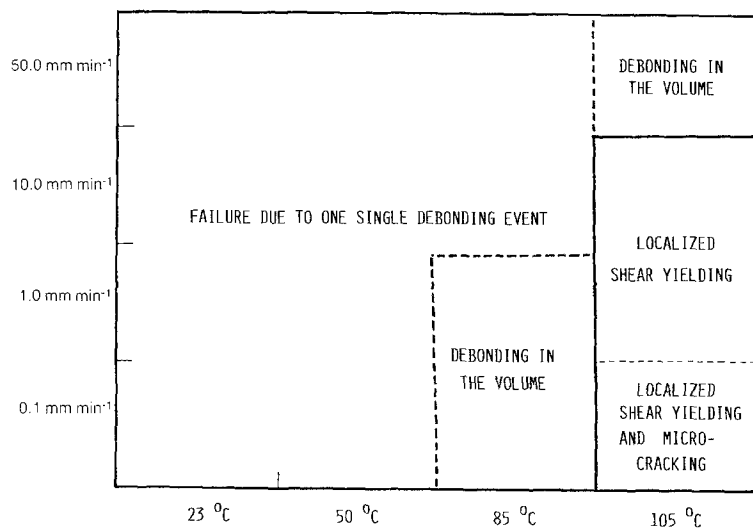


Figure 29 The dependence of localized shear yielding, particle-matrix debonding and micro-cracking on test temperature and cross-head speed.

increased strain in the matrix precipitated extensive volume damage which in turn influenced the process of crack propagation. Such damage is believed to degrade both the load-carrying capability as well as the toughness of the material.

Acknowledgements

The authors thank Dr A. C. Roulin-Moloney and Dr A. Demarmels for helpful suggestions and discussions, Jean-Luc Roulin for the technical assistance and Brian Senior (Institute Interdepartmental de

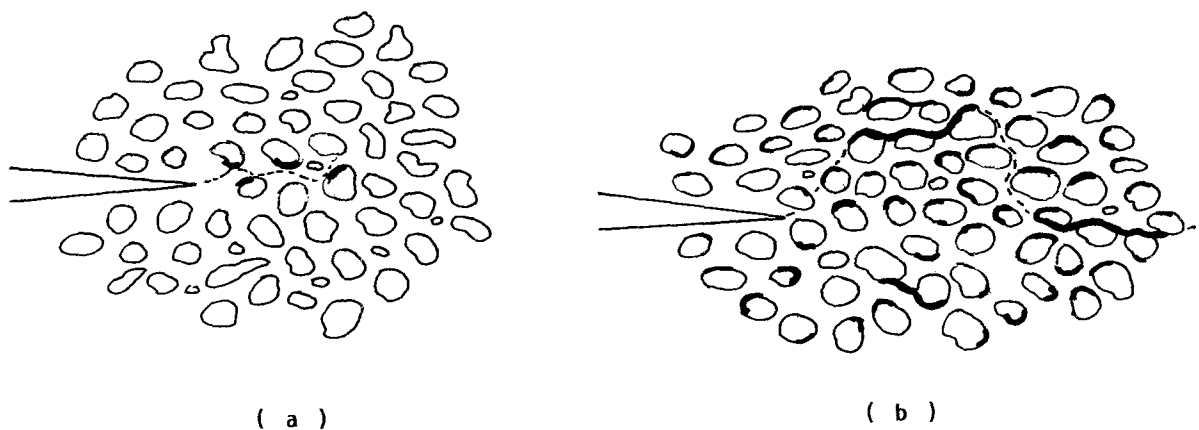


Figure 30 Schematic representations showing the process of crack extension which produce (a) a smooth sub-critical zone, (b) a rough sub-critical zone. The broken line shows the direction of anticipated crack growth.

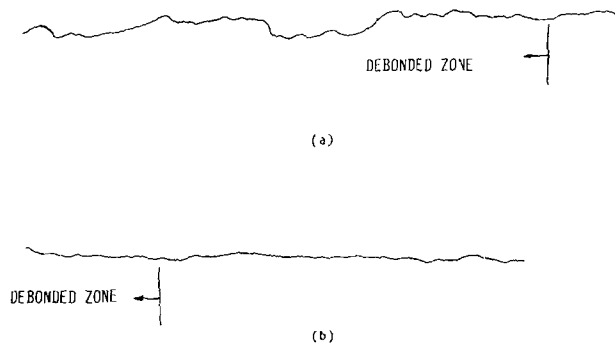


Figure 31 Reproductions showing the roughness of the sub-critical zone in specimens tested at (a) 0.1 mm min^{-1} , 105°C , and (b) 50 mm min^{-1} , 105°C .

Microscopie, EPFL) for help with the scanning electron microscopy. This work was financed by ASEA BROWN BOVERI Ltd and the Commission pour L'Encouragement de la Recherche Scientifique (CERS).

References

1. R. J. MORGAN and J. E. O'NEAL, *J. Mater. Sci.* **12** (1977) 1966.
2. J. LILLEY and D. G. HOLLOWAY, *Phil. Mag.* **28** (1973) 215.
3. M. KOGA, K. ASAMI and M. TERASAWA, Proceedings of the 21st Japanese Congress on Material Research (1978) p. 93.
4. B. W. CHERRY and K. W. THOMSON, *J. Mater. Sci.* **16** (1981) 1925.
5. R. E. ROBERTSON, V. E. MINDROIU and M. F. CHEUNG, *Comp. Sci. Tech.* **22** (1985) 197.
6. M. ATSUTA and D. T. TURNER, *J. Mater. Sci. Lett.* **1** (1982) 167.
7. A. S. WRONSKI and T. V. PARRY, *J. Mat. Sci.* **17** (1982) 2047.
8. M. KOGA, M. TAKASHI and S. KOIKE, Proceedings of the 27th Japanese Congress on Material Research (1984) p. 295.
9. W. J. CANTWELL, A. C. ROULIN-MOLONEY and T. KAISER, *J. Mater. Sci.* **23** (1988) 1615.
10. J. W. SMITH, T. KAISER and A. C. ROULIN-MOLONEY, *ibid.* **23** (1988) 3833.
11. A. S. HOLIK, R. P. KAMBOUR, P. G. FINK and S. Y. HOBBS, *Microstruct. Sci.* **7** (1979) 357.
12. J. W. SMITH, in "Fractography and Failure Mechanisms of Polymers and Composites", edited by A. C. Roulin-Moloney (Elsevier Applied Science, Barking, Essex, UK, 1988) Ch. 1.
13. A. G. EVANS, S. WILLIAMS and P. W. R. BEAUMONT, *J. Mater. Sci.* **20** (1985) 3668.
14. J. W. JOHNSON and D. G. HOLLOWAY, *Phil. Mag.* **14** (1966) 731.
15. J. N. PRICE and D. HULL, Proceedings of the 6th International Conference on Composite Materials and 2nd European Conference on Composite Materials, Vol. 4, edited by F. L. Matthews, N. C. R. Buskell, J. M. Hodgkinson and J. Morton (Elsevier Applied Science, Barking, Essex, UK, 1987) p. 365.
16. N. CUDRE-MAROUX, unpublished work, Lausanne (1987).
17. J. W. SMITH, unpublished work, Lausanne (1988).

Received 14 October 1988
and accepted 10 April 1989